Journal of Fluorescence, Vol. 11, No. 3, September 2001 (© 2001)

Single-Fluorophore Dynamic Imaging in Living Cells

Ryota Iino[1] and Akihiro Kusumi[1–3]

Recently, observation and tracking of single fluorophores, which we term single fluorophore dynamic imaging (SFDI) in this review, in living cells have been achieved. In particular, the recent success of SFDI of individual proteins tagged with green fluorescent protein (GFP) in live cells has opened new important possibilities for studying events occurring in living cells at the level of single molecules. Specifically, SFDI of GFP allows the tracking of movement and oligomerization levels of individual oligomers (monomers) in living cells and, thus, provides powerful means to investigate the movement, assembly, localization, and activation that signaling molecules undergo following an external stimulus. In this short account, we first review technologically important points for SFDI of GFP molecules in living cells, then give examples of its application, and, finally, propose a synergistic use of SFDI and single-particle tracking, a technique used for investigating single or small groups of molecules in live cells over the past 15 years.

KEY WORDS: Single-fluorophore imaging; green fluorescent protein; cell membrane; membrane skeleton; oligomer; translational diffusion.

INTRODUCTION

If we could observe the behavior (localization, transport, activation) of individual biomolecules of interest in living cells, it would be a great aid to the progress in cell biology. Recently, such investigations are becoming possible. Single-particle tracking (SPT) has allowed the tracking of individual molecules on the cell surface, contributing greatly to the understanding of the organization of the cell membrane [1–13]. In addition to SPT, recently, observation and tracking of single fluorophores [single-fluorophore dynamic imaging (SFDI)] in living cells have become possible [13–21]. Furthermore, very recently, SFDI of individual proteins conjugated with green fluorescent protein (GFP) in live cells has been achieved [16–21].

GFP technology is one of the fluorescence imaging methods that has contributed most to the recent progress in cell biology. GFP can be easily conjugated with proteins of interest at the cDNA level, and GFP-conjugated proteins can be easily expressed in live cells by transfection with cDNA plasmid [22]. Thus, labeling with GFP is a very powerful tool for the investigation of the behavior of proteins in living cells. However, until recently, SFDI of individual GFP-conjugated proteins was limited to isolated molecules *in vitro* [23–28]. The recent success of SFDI of GFP-conjugated proteins *in live cells* has extended new possibilities for studying events occurring in living cells at the level of single molecules.

OBJECTIVE-TYPE TOTAL INTERNAL REFLECTION FLUORESCENCE MICROSCOPY FOR SFDI

SFDI in an aqueous environment can be achieved by (1) confocal laser scanning microscopy [28–35], (2)

[1] Kusumi Membrane Organizer Project, Exploratory Research for Advanced Technology Organization (ERATO), Japan Science and Technology Corporation, Chiyoda 5-11-33, Nagoya 460-0012, Japan.
[2] Department of Biological Science, Nagoya University, Nagoya 464-8602, Japan.
[3] To whom correspondence should be addressed at Department of Biological Science, Nagoya University, Nagoya 464-8602, Japan. Fax: +81-52-789-2968. E-mail: akusumi@bio.nagoya-u.ac.jp

1053-0509/01/0900-0187$19.50/0

low-background epifluorescence microscopy [15,17, 18,20,36–42], and (3) total internal reflection fluorescence microscopy (TIRFM) [14,16,19,21,23–26,42–47]. With confocal laser scanning microscopy, Mets and Rigler [29] and Nie *et al.* [30] were the first to achieve detection of single fluorescent dye molecules in aqueous solutions. Sase *et al.* [39] and Funatsu *et al.* [42] first succeeded in single fluorophore imaging of biomolecules *in vitro* using low-background epifluorescence microscopy and TIRFM. In particular, Funatsu *et al.* [42] compared the same image field using both optical and electron microscopy and showed unequivocally that observation of single fluorescent molecules in solution using optical microscopy is possible. Because of this work, SFDI in aqueous solutions has been accepted as possible. In this regard, this work is the most important among the early SFDI research.

Among the methods described above, TIRFM has been used frequently for SFDI [14,16,19,21,23–26,42–47]. Recently, objective-type TIRFM [45,48] is becoming popular, because the optics of the instrument can be set up easily, and the geometric configuration around the sample is simplified to allow the use of, in addition to TIRFM and normal epifluorescence microscopy, transmission light microscopy and easy access to the sample for micromanipulation, microinjection, and scanning for atomic force microscopy. SFDI with objective-type TIRFM has become possible by manufacturers' effort to reduce greatly the light scattering and fluorescence emitted by the microscope when laser light is introduced into the microscope. Objective-type TIRFM was first proposed by Axelrod [48] and first applied to SFDI by Tokunaga *et al.* [45].

Figure 1A shows the objective-type TIRFM system used for observations of GFP in live cells in our laboratory [16,21]. GFP molecules are excited with an evanescent field formed by the total internal reflection of a 488-nm-wavelength argon-ion laser beam. The fluorescence images are projected onto a microchannel plate intensifier coupled (by relay lens) to a silicon-intensified target tube (SIT) camera and are recorded at the video rate by a digital video cassette recorder. In TIRFM, the excitation volume is limited to a thin layer of a typical thickness of 100–200 nm on and above the glass surface [48], and thereby background signals in solution due to Raman scattering, Rayleigh scattering, and fluorescence are greatly reduced. TIRFM is suitable for the observation of events near the portion of the plasma membrane adhered to the coverslip. In addition, Sako *et al.* [14] found that TIRFM is possible at the interface of the cell and the extracellular solvent, i.e., at the cell membrane facing the culture medium (rather than the coverslip,

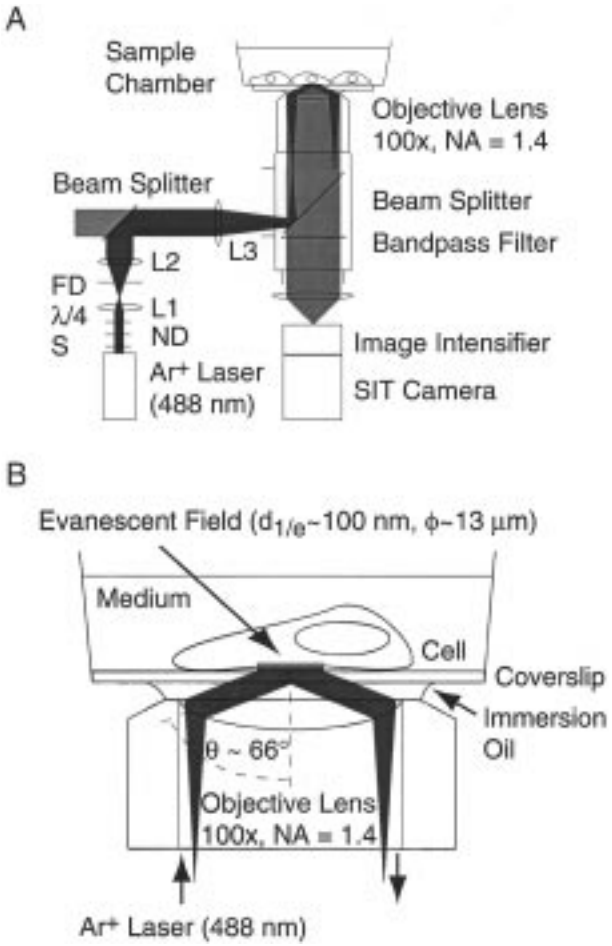

Fig. 1. The objective-type TIRFM system used in our laboratory. (A) Optical ray diagram. A 488-nm argon-ion laser beam is expanded by two lenses (L1 and L2) and focused at the back-focal plane of the objective lens with another lens (L3). S, ND, λ/4, and FD represent the electronic shutter, neutral density filter, quarter-wave plate, and field diaphragm, respectively. (B) Schematic drawing of the sample chamber and the objective lens. An evanescent field is formed (thickness, about 100 nm) on the coverslips by the total internal reflection of a laser beam. The diameter of the illuminated area is about 13 μm.

dorsal surface or apical surface). We confirmed that single-GFP molecule imaging on the dorsal cell surface at the video rate is possible, although we are not totally sure if total internal reflection is occurring at the cell–external solvent interface.

Figure 1B shows a schematic drawing of the sample chamber and the objective lens. For observations of single GFP molecules in living cells, we have made the following modifications to the system used by Tokunaga *et al.* [45], to reduce further the autofluorescence signal from the cell: (1) the incident angle of the laser was set relatively large (about 66°), and the thickness of the evanescent field ($d_{1/e}$) was reduced to approximately 100 nm;

and (2) the illuminated area on the coverslip was reduced to approximately 130 μm^2 (13 μm in diameter).

IMAGING OF SINGLE GFP-CONJUGATED PROTEINS IN LIVING CELLS

Using objective-type TIRFM, we have succeeded in SFDI of GFP-conjugated proteins in living cells [16,21]. In this review, we concentrate mostly on the observation of GFP fused with E-cadherin (E-cad-GFP) as an example, because it appears to be the only case of SFDI of GFP-conjugated proteins in live cells which has appeared in a peer-reviewed journal thus far. However, several meeting abstracts and proceedings indicate that other groups have also succeeded in observations of GFP-conjugated molecules in live cells [16–21]. Lommerse *et al.* [18] observed individual yellow fluorescent protein (YFP; a red-shifted variant of GFP) conjugated to the C-terminus domain of H-ras (YFP-CAAX) in tsA301 cells. This molecule binds to the inner leaflet of the cell membrane via farnesylation and palmitoylation of the C-terminus domain. About half of the YFP-CAAX molecules exhibited confined diffusion within domains having an average diameter of 190 nm, and the rest exhibited simple diffusion having a mean diffusion coefficient of 1.3 $\mu m^2/s$. Furthermore, in a very recent publication in a peer-reviewed journal, Harms *et al.* [20] reported that they were able to observe and track individual phospholipid molecules conjugated to single YFP via nickel-ion chelating groups in the plasma membrane of human aorta smooth muscle cells, although the mean photobleaching time is extremely short (2–4 ms).

E-Cadherin is responsible for Ca^{2+}-dependent cell–cell adhesion in epithelial and several other tissues. E-cad-GFP molecules were expressed in mouse fibroblast L cells (we refer to the L cells expressing E-cad-GFP as LEG cells in this review). In SFDI of GFP-conjugated molecules, the cells expressing low levels of GFP-fusion protein should be selected, because the fluorescence spots from molecules present at higher concentrations overlap each other, making SFDI impossible. For example, we used LEG cells expressing E-cad-GFP at less than 1% of the average level of endogenous E-cadherin expressed in Madin–Darby canine kidney (MDCK) epithelial cells. For easy culturing and TIRFM observation of cells, glass-bottom culture dishes are highly suitable. Since it is critical to remove the dust and other impurities from the glass surface and other parts of the chamber, we recommend sonication of glass-bottom dishes in a 0.1 *M* NaOH solution for 90 min before cell culture and observation. Furthermore, cells should be kept under good proliferative conditions, because unfavorable conditions tend to lead to an increase in autofluorescence in the cytoplasm and fluorescent debris (perhaps containing GFP) released from the dead cells.

When the cells expressing low levels of E-cadherin were observed, individual spots could be discerned after about 50% of the E-cad-GFP was photobleached. Figure 2A shows a fluorescence image of the LEG cell acquired 3 s after the excitation light was turned on (at which 50% of the E-cad-GFP was photobleached). Under these conditions, E-cad-GFP molecules were observed as many spots with various fluorescence intensities. In contrast, autofluorescence of L cells was low (Fig. 2B). These results are compared quantitatively in Fig. 2C, in which the average fluorescence intensity in an image area (5.8×5.8 μm) is shown as a function of the time after the start of excitation. The solid and dashed lines in Fig. 2C show the decay of fluorescence intensities by photobleaching for LEG and L cells, respectively. The autofluorescence intensity of L cells was less than 10% of the fluorescence intensity of the LEG cells when compared immediately after the initiation of the observation (Fig. 2C, near time 0).

Spots of E-cad-GFP had various fluorescence intensities. To quantitate such variations, we first measured the background signal intensities in small areas (408×408 nm) of L cells by randomly selecting the positions. This intensity includes autofluorescence from the cell, stray excitation light (which passed the emission selecting filters), fluorescence from the optical system, and the thermal noise of the detector and the electronic system. The intensity distribution of the background signal is shown in Fig. 3A, and its mean value of 7.6 arbitrary units (AU; $N = 625$) was subtracted in all histograms in Fig. 3. The histograms for the fluorescence intensity of E-cad-GFP spots measured after 50% photobleaching showed a quantized distribution with a basic fluorescence intensity of about 16 AU ($N = 326$) (Fig. 3B). As a control experiment, we observed purified GFP molecules. The fluorescence intensities of individual GFP molecules nonspecifically attached to the cell surface or the coverslip were comparable (15 AU; $N = 110$) (Fig. 3C) or slightly higher (20 AU, $N = 110$) (Fig. 3D), respectively, to that of the basal peak of E-cad-GFP molecules. The higher intensity of GFP fluorescence on the coverslip is due to the short distance from the GFP fluorophore to the coverslip–medium interface, since the intensity of the evanescent field decays exponentially as a function of the distance from the interface [48]. Furthermore, E-cad-GFP spots with fluorescent intensities of the basal peak (indicated by arrows in Fig. 4A) showed single-step, quantized photobleaching (Fig. 4B). From these results, it

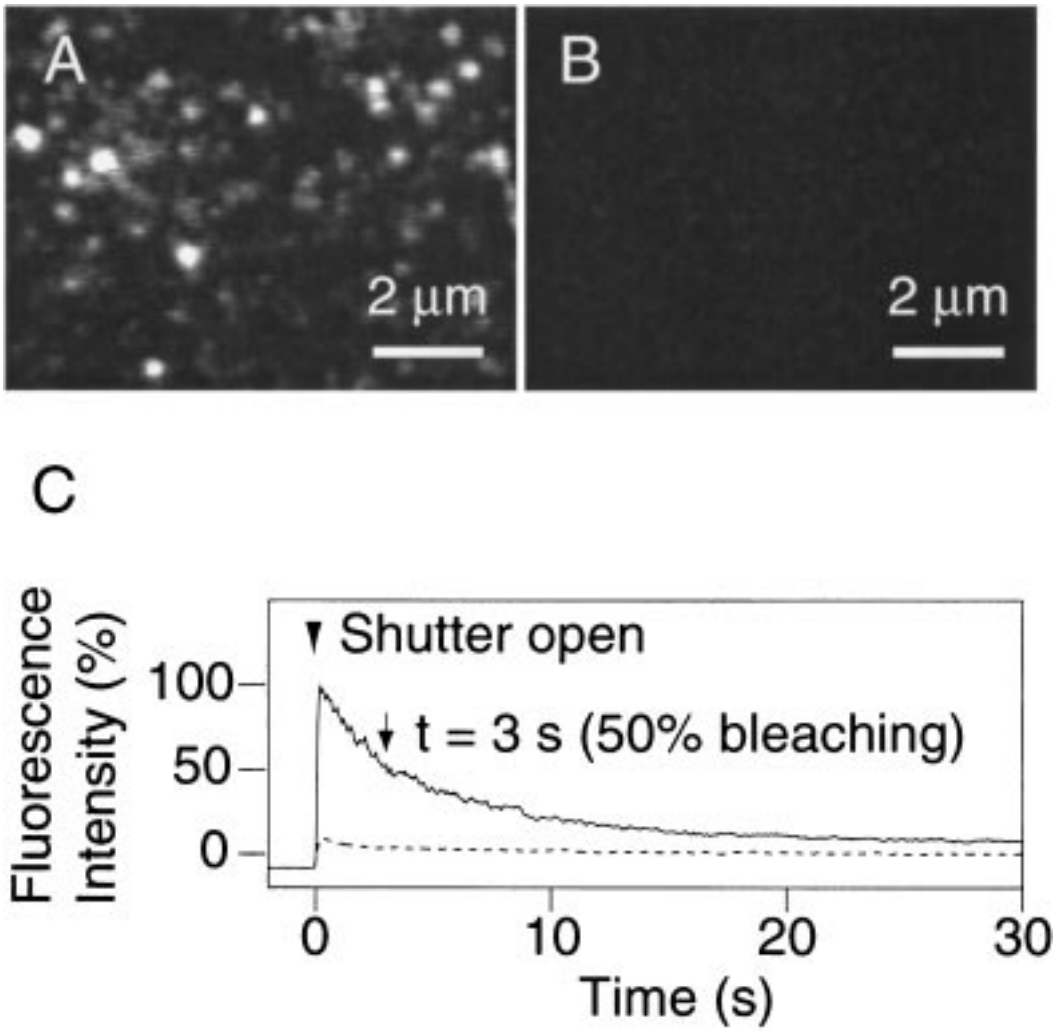

Fig. 2. SFDI of E-cad-GFP on the ventral membrane of a LEG cell. (A, B) Images of a LEG cell (A) and a control L cell (B) acquired after 50% photobleaching of E-cad-GFP (t = 3 s in C). (C) Typical decays of the fluorescence intensity in a LEG cell and an L cell by photobleaching in 5.8 × 5.8-μm areas. Solid line, LEG cell; dashed line, L cell.

is concluded that E-cad-GFP molecules were individually imaged in live cells.

DETECTION OF E-CAD-GFP OLIGOMERS

The presence of many quantized peaks in the distribution of fluorescence intensities of E-cad-GFP on the LEG cell surface suggests that many E-cad-GFP molecules form oligomers, even on the free surface outside the sites of cell–cell adhesion (Fig. 3B). The presence of various sizes of E-cadherin oligomers was observed for the first time by performing SFDI on GFP-conjugated E-cadherin in living cells. As such, SFDI of GFP-conjugated proteins allows the detection of oligomer formation and estimation of the oligomerization level. Since dimerization and further oligomerization of receptor molecules and of intracellular signaling molecules [49,50] in and on the cell membrane are critical steps for signal transduction there, SFDI of GFP-conjugated proteins in living cells would provide a useful tool for the investigation of signaling processes in the cell membrane. However, one would have to be careful about GFP-induced oligomerization, particularly when the expression level of GFP-conjugated protein is high. In the case of E-cad-GFP, even when its expression level is kept lower than 1% of that of the endogenous E-cadherin expressed in MDCK epithelial cells, oligomers greater than dimers were observed.

Furthermore, the movement of individual molecules can be tracked. We found that fluorescent spots with

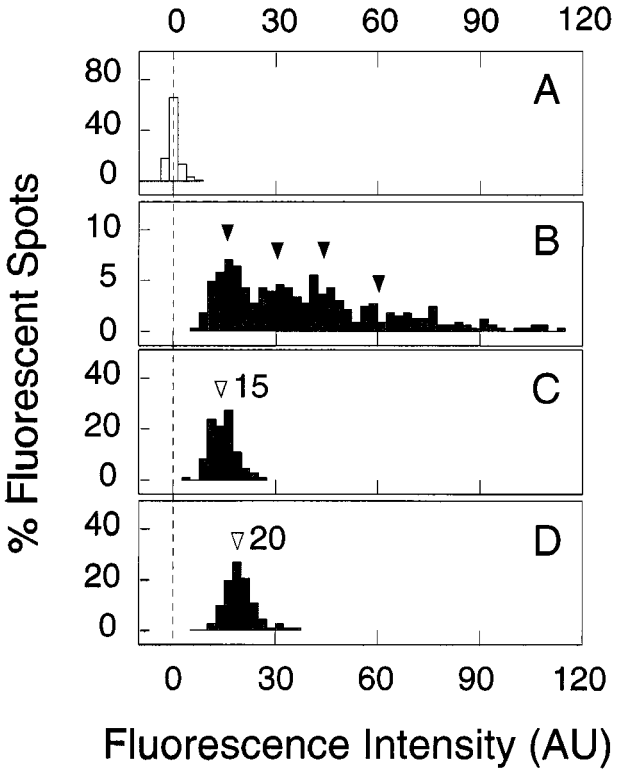

Fig. 3. Quantized distribution of the fluorescence intensity of E-cad-GFP. Histograms of fluorescence intensities within areas (408 × 408 nm) containing a single spot are shown. The mean value of the background intensity for the L cell (7.6 AU) was subtracted from all histograms. (A) Distribution of the background intensity of L cells. (B) Distribution of the fluorescence intensities of E-cad-GFP spots after 50% photobleaching. Filled arrowheads indicate quantized peaks. (C, D) Distributions of the fluorescence intensity of purified GFP molecules attached to the membrane of the L cell (C) or the coverslip (D). Open arrowheads indicate mean values. AU, arbitrary units.

various intensities undergo translational diffusion without splitting. Therefore, spots with fluorescence intensities greater than those of monomers do not simply indicate two or more E-cad-GFP molecules present within distances closer than the optical diffraction limit but, in fact, represent true oligomers of E-cad-GFP. Even when fluorescent intensities are measured after photobleaching, the intensity distribution could provide a convenient estimate for the degree of oligomerization. In the case of E-cad-GFP in LEG cells, the oligomerization level is expected to be less than decamers, since spots with intensities greater than that of dimers were rarely observed after 80% photobleaching [16,21]. However, since the expression level of E-cad-GFP in LEG cells was very low, we suspect that larger oligomers may be formed in the plasma membrane of cells naturally expressing higher levels of wild-type E-cadherin.

RELATION BETWEEN THE E-CAD-GFP OLIGOMERIZATION LEVEL AND ITS TRANSLATIONAL MOBILITY

As described above, the oligomerization level and movement of GFP-conjugated proteins in live cells can be investigated simultaneously using SFDI. Figure 5 shows E-cad-GFP fluorescence spots with different intensities and their trajectories for 5 s. The movement was tracked at the video rate with 20-nm positional accuracy. As the fluorescence intensity increased, the trajectories tended to exhibit less motion. Figure 6 shows the relationship between the diffusion coefficient and the fluorescence intensity of each spot. In Fig. 6, the boundaries between different quantized intensities determined by the peaks shown in Fig. 3B are indicated by dashed vertical lines. Although these quantized intensities do not repre-

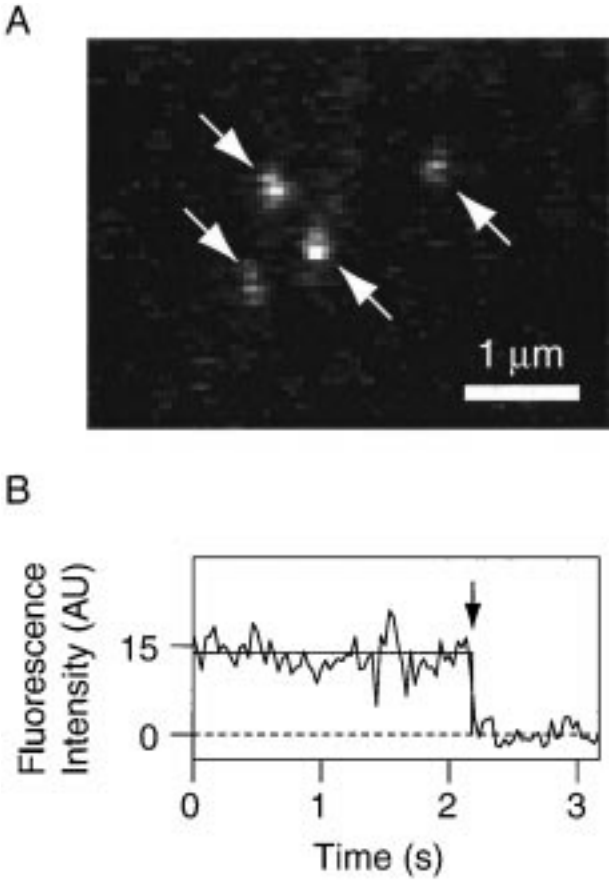

Fig. 4. E-cad-GFP spots with basic quantized intensities show single-step photobleaching. (A) An image of E-cad-GFP spots with basic quantized intensities (indicated by arrows). (B) A typical example of the change in fluorescence intensity of an E-cad-GFP spot with a basic quantized intensity observed at the video rate. Single-step photobleaching occurred at the time indicated by the arrow. AU, arbitrary units.

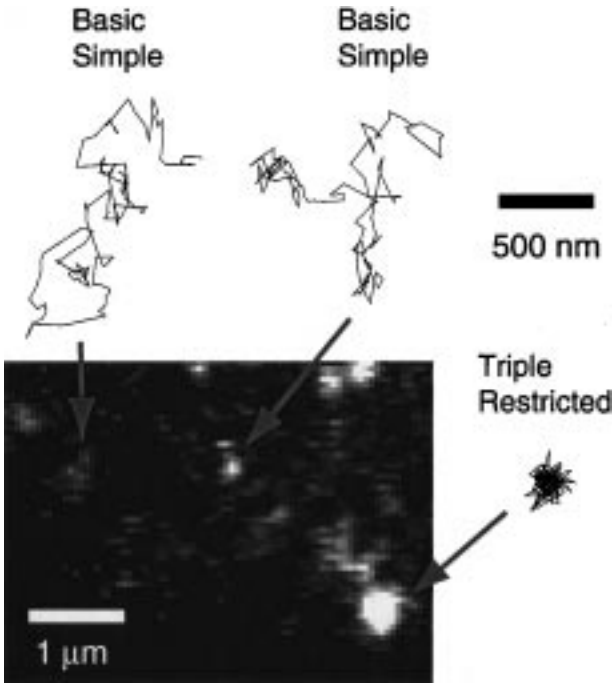

Fig. 5. E-cad-GFP spots with higher fluorescence intensities show more restricted motion. A fluorescence image of E-cad-GFP spots with basic or triple quantized intensities and their trajectories for 5 s (150 video frames) are shown. Above each trajectory, the quantized intensity (basic or triple) and the motional mode (simple or restricted) of each spot are indicated.

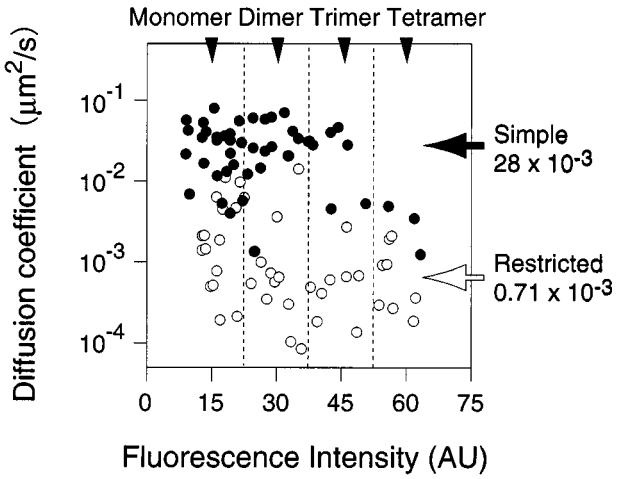

Fig. 6. E-cad-GFP spots with higher fluorescence intensities exhibit much lower diffusion rates and a restricted mode of diffusion. The diffusion coefficient and the fluorescence intensity of each spot are plotted. Each spot was classified either into the simple (filled circles) or the restricted (open circles) diffusion mode and the four apparent oligomerization levels (monomer to tetramer as divided by dashed lines). Filled and white arrows indicate the median values of the diffusion coefficients for each diffusion mode. AU, arbitrary units.

sent the actual oligomer size because of photobleaching, they provide a convenient yardstick for the degree of oligomerization. The spots with monomer intensity tended to have a higher fraction of simple diffusion (filled circles) and higher diffusion rates. In contrast, spots with greater oligomerization levels have a higher fraction of restricted diffusion (open circles) and lower diffusion rates (Fig. 6). The median diffusion coefficients of spots undergoing simple and restricted diffusion were 28×10^{-3} and 0.71×10^{-3} $\mu m^2/s$, respectively, a difference of a factor of 40. Since translational diffusion in a two-dimensional fluid is very *insensitive* to changes in the size of the diffusing unit [51], this result indicates the presence of a mechanism by which movement of E-cad-GFP oligomers on the free cell surface is very effectively suppressed.

OLIGOMERIZATION-INDUCED TRAPPING OF MEMBRANE PROTEINS IN THE MEMBRANE SKELETON MESHES

The membrane skeleton provides both the binding (tethering) and the confining effects on transmembrane proteins (Fig. 7) [3–13]. Transmembrane proteins tethered to the membrane skeleton are immobile, and even those that are not directly bound to the membrane skeleton

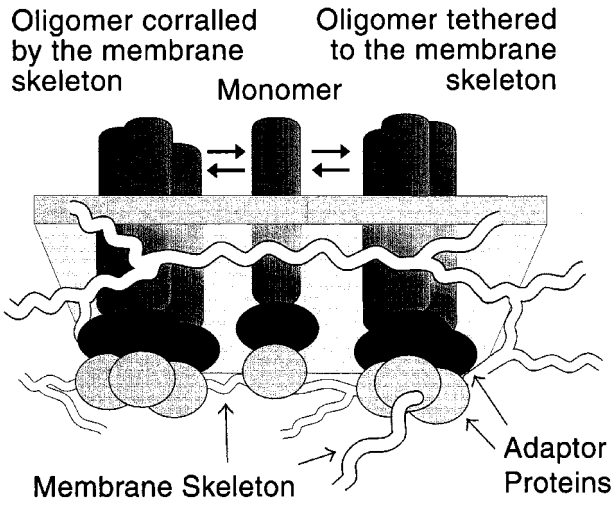

Fig. 7. An oligomerization-induced trapping model, in which a strong coupling of the oligomerization of transmembrane proteins with the membrane skeleton's tethering and corraling effects is proposed. (Left) Oligomers tend to "hop" to an adjacent compartment much more slowly than monomers because they have greater cytoplasmic domains. (Center) Monomers are relatively free of tethering to the membrane skeleton and can readily "hop" the membrane skeleton. (Right) Oligomers are much more likely to be tethered to the membrane skeleton due to multivalency (avidity) effects.

are temporarily confined (~1-s level) in submicron compartments formed by the membrane skeleton meshes and occasionally "hop" to an adjacent compartments. By repeating such hop movements, the transmembrane proteins undergo macroscopic diffusion.

Oligomerization of a membrane protein greatly increases these effects of the membrane skeleton. Based on the observation that oligomerized E-cad-GFP exhibits greatly reduced translational diffusion, we propose an "oligomerization-induced trapping model" (Fig. 7), in which transmembrane receptors are trapped and immobilized where the oligomerization occurrs due to increased interactions with the membrane skeleton [16,21]. Since greater oligomers have larger cytoplasmic portions compared with monomers, they have much less chance of "hopping" and tend to exhibit restricted diffusion. Furthermore, greater oligomers are more likely to be immobilized by tethering to the membrane skeleton since every monomer in the oligomer must dissociate from the membrane skeleton before the oligomer itself can detach.

It is well known that many receptor molecules form oligomers during their signal transduction [52,53]. Our model could be particularly important for understanding receptor-mediated signaling processes that induce the polarized response of a cell. In these kinds of signaling, cells must "memorize" the point that the extracellular signal has reached. Cells may accomplish this by immobilizing the activated receptor by increasing the oligomerization level, causing it to be trapped in place by the membrane skeleton.

SFDI OF CHEMICAL DYE MOLECULES IN LIVING CELLS

Because chemical dye molecules have a higher quantum efficiency, molecular extinction coefficient, and photostability, in general, SFDI in living cells can be carried out more easily if proteins of interest can be tagged with these dye molecules in live cells. Cell surface molecules can be labeled with fluorescently tagged antibodies or ligands. Fluorescently tagged lipids and glycosylphosphatidylinositol-anchored proteins can be incorporated in the cell membrane when they are added from outside the cell. Intracellular proteins, after being artificially expressed in some cells and purified, can be labeled *in vitro* with a chemical dye and then introduced into the cytoplasm by microinjection or by temporarily injuring the cell membrane [54–56]. Since these processes tend to be cumbersome, we generally prefer first testing the effectiveness of GFP, and then if we find a good reason to switch to chemical dyes, such as the need to improve the signal-to-noise ratio or the necessity to observe for a longer period, we do so. Several important results have been obtained employing fluorescently tagged proteins for investigations using live cells.

Using objective-type TIRFM, Sako *et al.* [14] carried out SFDI of Cy3-conjugated epidermal growth factor (Cy3-EGF) attached to the cell surface and investigated the signal transduction process mediated by the EGF receptor (EGFR) on the surface of A431 carcinoma cells. Tracking of single Cy3-EGF revealed that EGF molecules in solution preferentially bind to high-affinity-type EGFR, which are likely to be preformed dimers or a complex of an EGF-bound EGFR molecule and an unoccupied EGFR molecule. Dimerization of EGFR was further confirmed by observing the fluorescence resonance energy transfer (FRET) from a single Cy3-EGF molecule to a single Cy5-EGF molecule bound to EGFR.

Schütz *et al.* [15] carried out an SFDI of Cy5-labeled lipids in human coronary artery smooth muscle cells with a millisecond time resolution and 50-nm positional accuracy using low-background epifluorescence microscopy. Although their instrument setup allowed them to obtain only 14 successive images, the membrane domains were detected by observing Cy5-conjugated phosphatidylethanolamine with saturated myristoyl chains (DMPE-Cy5) and were shown to be small compartments (0.7 μm in diameter) likely having liquid-ordered phase properties. DMPE-Cy5 was highly partitioned into such domains and stayed for an average of 13 s. Although the movement of DMPE was confined, its diffusion rate within the domain was not reduced (0.6 $\mu m^2/s$). An analogous Cy5-labeled lipid with diunsaturated chains (DOPE-Cy5) did not exhibit such confined-type diffusion.

COMPARISON OF SINGLE-PARTICLE TRACKING (SPT) AND SFDI

In SPT, the movement of small colloidal gold or latex particles, which are attached either to single or to a small number of proteins of interest via their ligands or the antibodies' Fab fragments, is tracked. Prior to the advent of SFDI, SPT was applied to studies of events occurring in living cells. The most important advantage of SFDI over SPT is that labeling of the target protein with a single probe (fluorophore) can be achieved much more easily than with larger gold or latex particles [7,13,57]. Most proteins adsorbed on the colloidal gold surface are denatured (becoming incapable of binding to the target proteins) or have wrong orientations for binding to the target molecules. Under these conditions, making probes that bind specifically to the target molecules with-

out cross-linking them is not an easy task. Other advantages of SFDI over SPT include the following: (1) due to the small size of the probe (although GFP has a diameter of about 4 nm), the steric hindrance in the cell is expected to be small; (2) the degree of oligomerization can be estimated with GFP-fused proteins [16,21]; (3) the formation of molecular complexes can be detected by single-molecule FRET [14,28,32–35,47,57,59–61]; and (4) the orientation and reorientation of a molecule can be detected by single-molecule fluorescence polarization measurements [20,39,41,57,58,60].

On the other hand, SPT has two major advantages over SFDI: (1) observations for long durations (up to several tens of minutes) are possible (in SFDI, the duration is limited to 1–20 s due to photobleaching), and (2) the high signal-to-noise ratio of SPT allows high time resolutions. We have succeeded in SPT of colloidal gold particles (40 nm in diameter) in live cells at a 25-μs time resolution (which is better than the normal video's time resolution by a factor of 1300) [10,12]. These advantages of SPT have been essential for investigation of the regulation mechanism of the movement of membrane proteins in the cell membrane. Further, one of the great bonuses of using SPT is provided by its combination with optical tweezers. Since colloidal gold or latex particles can be trapped and dragged with optical tweezers, the interaction force between molecules can be measured, and consequences following the forced assembly or dissociation of molecules (using optical tweezers) can be investigated in live cells. Because of the distinct characteristics of SPT and SFDI, they can be used complimentarily and synergistically. It is important to understand the advantages and drawbacks of SPT and SFDI and to use the method that suits one's particular experimental purpose.

Most biomolecular systems work stochastically. A molecule's environment, conformational state, and interactions with other molecules are intrinsically inhomogeneous and change asynchronously within a cell, and only small populations of a molecule in a cell may respond to a particular stimulus. Therefore, although it may sound paradoxical, single-molecule technologies are important for studying complex molecular systems such as a cell. Single-molecule technologies may in fact provide the only possibility for overcoming intrinsically stochastic and inhomogeneous properties of biological molecular systems in investigations for understanding their working mechanisms. SFDI in living cells will become one of the most important tools for single-molecule analysis, especially when it is coupled with GFP technology.

REFERENCES

1. M. De Brabander, G. Geuens, R. Nuydens, M. Moeremans, and J. De Mey (1985) *Cytobios* **43**, 273–283.
2. J. Gelles, B. J. Schnapp, and M. P. Sheetz (1988) *Nature* **331**, 450–453.
3. A. Kusumi, Y. Sako, and M. Yamamoto (1993) *Biophys. J.* **65**, 2021–2040.
4. Y. Sako and A. Kusumi (1994) *J. Cell Biol.* **125**, 1251–1264.
5. E. D. Sheets, R. Simson, and K. Jacobson (1995) *Curr. Opin. Cell Biol.* **7**, 707–714.
6. Y. Sako and A. Kusumi (1995) *J. Cell Biol.* **129**, 1559–1574.
7. A. Kusumi and Y. Sako (1996) *Curr. Opin. Cell Biol.* **8**, 566–574.
8. M. J. Saxton and K. Jacobson (1997) *Annu. Rev. Biophys. Biomol. Struct.* **26**, 373–399.
9. Y. Sako, A. Nagafuchi, S. Tsukita, M. Takeichi, and A. Kusumi (1998) *J. Cell Biol.* **140**, 1227–1240.
10. M. Tomishige, Y. Sako, and A. Kusumi (1998) *J. Cell Biol.* **142**, 989–1000.
11. A. Kusumi, K. Suzuki, and K. Koyasako (1999) *Curr. Opin. Cell Biol.* **11**, 582–590.
12. M. Tomishige and A. Kusumi (1999) *Mol. Biol. Cell.* **10**, 2475–2479.
13. G. J. Schütz, M. Sonnleitner, P. Hinterdorfer, and H. Schindler (2000) *Mol. Membr. Biol.* **17**, 17–29.
14. Y. Sako, S. Minoghchi, and T. Yanagida (2000) *Nature Cell Biol.* **2**, 168–172.
15. G. J. Schütz, G. Kada, V. Ph. Pastushenko, and H. Schindler (2000) *EMBO J.* **19**, 892–901.
16. R. Iino, I. Koyama, and A. Kusumi (2000) *Cell Struct. Funct.* **25**, 472.
17. G. S. Harms, L. Cognet, P. H. M. Lommerse, G. A. Blab, E. Snaar-Jagalska, C. Romanin, N. Soldatov, H. P. Spaink, and T. Schmidt (2001) *Biophys. J.* **80**, 151a.
18. P. H. M. Lommerse, L. Cognet, G. A. Blab, G. S. Harms, E. Snaar-Jagalska, H. P. Spaink, and T. Schmidt (2001) *Biophys. J.* **80**, 153a.
19. A. Sonnleitner, S. Licht, X. Michalet, P. G. Schultz, and S. Weiss (2001) *Biophys. J.* **80**, 201a.
20. G. S. Harms, L. Cognet, P. H. M. Lommerse, G. A. Blab, and T. Schmidt (2001) *Biophys. J.* **80**, 2396–2408.
21. R. Iino, I. Koyama, and A. Kusumi (2001) *Biophys. J.* **80**, 2667–2677.
22. K. F. Sullivan and S. A. Kay (Eds.) (1999) *Green Fluorescent Proteins*, Academic Press, San Diego.
23. D. W. Pierce, N. Hom-Booher, and R. D. Vale (1997) *Nature* **388**, 338.
24. R. M. Dickson, A. B. Cubitt, R. Y. Tsien, and W. E. Moerner (1997) *Nature* **388**, 355–358.
25. A. H. Iwane, T. Funatsu, Y. Harada, M. Tokunaga, O. Ohara, S. Morimoto, and T. Yanagida (1997) *FEBS Lett.* **407**, 235–238.
26. L. Romberg, D. W. Pierce, and R. D. Vale (1998) *J. Cell Biol.* **140**, 1407–1416.
27. U. Kubitscheck, O. Kückmann, and R. Peters (2000) *Biophys. J.* **78**, 2170–2179.
28. S. Brasselet, E. J. G. Peterman, A. Miyawaki, and W. E. Moerner (2000) *J. Phys. Chem.* **104**, 3676–3682.
29. U. Mets and R. Rigler (1994) *J. Fluoresc.* **4**, 259–264.
30. S. Nie, D. T. Chiu, and R. N. Zare (1994) *Science* **11**, 1018–1021.
31. H. P. Lu, L. Xun, and X. S. Xie (1998) *Science* **282**, 1877–1882.
32. T. Ha, A. Y. Ting, J. Liang, W. B. Caldwell, A. A. Deniz, D. S. Chemla, P. G. Schultz, and S. Weiss (1999) *Proc. Natl. Acad. Sci. USA* **96**, 893–898.
33. A. A. Deniz, M. Dahan, J. R. Grunwell, T. Ha, A. E. Faulhaber, D. S. Chemla, S. Weiss, and P. G. Schultz (1999) *Proc. Natl. Acad. Sci. USA* **96**, 3670–3675.
34. T. Ha, X. Zhuang, H. D. Kim, J. W. Orr, J. R. Williamson, and S. Chu (1999) *Proc. Natl. Acad. Sci. USA* **96**, 9077–9082.
35. A. A. Deniz, T. A. Laurence, G. S. Beligere, M. Dahan, A. B. Martin, D. S. Chemla, P. E. Dawson, P. G. Schultz, and S. Weiss (1999) *Proc. Natl. Acad. Sci. USA* **97**, 5179–5184.
36. I. Sase, H. Miyata, J. E. Corrie, J. S. Craik, and K. Kinosita Jr. (1995) *Biophys. J.* **69**, 323–328.
37. Th. Schmidt, G. J. Schütz, W. Baumgartner, H. J. Gruber, and H. Schindler (1995) *J. Phys. Chem.* **99**, 17662–17668.

38. Th. Schmidt, G. J. Schütz, W. Baumgartner, H. J. Gruber, and H. Schindler (1996) *Proc. Natl. Acad. Sci. USA* **93**, 2926–2929.
39. I. Sase, H. Miyata, S. Ishiwata, and K. Kinosita, Jr. (1997) *Proc. Natl. Acad. Sci. USA* **94**, 5646–5650.
40. Y. Okada and N. Hirokawa (1999) *Science* **283**, 1152–1157.
41. K. Adachi, R. Yasuda, H. Noji, H. Itoh, Y. Harada, M. Yoshida, and K. Kinosita Jr. (2000) *Proc. Natl. Acad. Sci. USA* **97**, 7243–7247.
42. T. Funatsu, Y. Harada, M. Tokunaga, K. Saito, and T. Yanagida (1995) *Nature* **374**, 555–559.
43. R. D. Vale, T. Funatsu, D. W. Pierce, L. Romberg, Y. Harada, and T. Yanagida (1996) *Nature* **380**, 451–453.
44. R. M. Dickson, D. J. Norris, Y. L. Tzeng, and W. E. Moerner (1996) *Science* **274**, 966–969.
45. M. Tokunaga, K. Kitamura, K. Saito, A. H. Iwane, and T. Yanagida (1997) *Biochem. Biophys. Res. Commun.* **235**, 47–53.
46. X. H. Xu and E. S. Yeung (1997) *Science* **275**, 1106–1109.
47. X. Zhuang, L. E. Bartley, H. P. Babcock, R. Russell, T. Ha, D. Herschlag, and S. Chu (2000) *Science* **288**, 2048–2051.
48. D. Axelrod (1989) *Methods Cell Biol.* **30**, 245–270.
49. M. A. Farrar, J. Alberola-Ila, and R. M. Perlmutter (1996) *Nature* **383**, 178–181.
50. Z. Luo, G. Tzivion, P. J. Belshaw, D. Vavvas, M. Marshall, and J. Avruch (1996) *Nature* **383**, 181–185.
51. P. G. Saffman and M. Delbrück (1975) *Proc. Natl. Acad. Sci. USA* **72**, 3111–3113.
52. T. E. Hébert and M. Bouvier (1998) *Biochem. Cell Biol.* **76**, 1–11.
53. J. Schlessinger (2000) *Cell* **103**, 211–225.
54. P. L. McNeil, R. F. Murphy, F. Lanni, and D. L. Taylor (1984) *J. Cell Biol.* **98**, 1556–1564.
55. P. L. McNeil and E. Warder (1987) *J. Cell Sci.* **88**, 669–678.
56. J. A. Swanson and P. L. McNeil (1987) *Science* **238**, 548–550.
57. S. Weiss (1999) *Science* **283**, 1676–1683.
58. T. Ha, Th. Enderle, D. S. Chemla, P. R. Selvin, and S. Weiss (1996) *Phys. Rev. Lett.* **77**, 3979–3982.
59. T. Ha, T. Enderle, D. F. Ogletree, D. S. Chemla, P. R. Selvin, and S. Weiss (1996) *Proc. Natl. Acad. Sci. USA* **93**, 6264–6268.
60. S. Weiss (2000) *Nature Struct. Biol.* **7**, 724–729.
61. A. A. Deniz, T. A. Laurence, M. Dahan, D. S. Chemla, P. G. Schultz, and S. Weiss (2001) *Annu. Rev. Phys. Chem.* **52**, 233–253.